Supplemental Data

If not specified, reagents were purchased from Sigma-Aldrich, a Merck company.

Cell lines and treatment

The $SSTR_2$-positive human small cell lung cancer cell line NCI-H69 and the neuroendocrine tumor cell line GOT1 were obtained from the American Type Culture Collection (ATCC) and Prof. Ola Nilsson (Sahlgrenska Cancer Center, University of Gothenburg, Sweden), respectively. GOT1 cells were maintained in RPMI 1640 (Gibco), supplemented with 10% fetal calf serum (FCS; Biowest), 1% penicillin-streptomycin (PS; Sigma-Aldrich), 5 mM L-glutamine (Stemcell Technologies), 5 µg/mL insulin (Sigma) and 5 µg/mL human holo-transferrin (Sigma). NCI-H69 cells were cultured in RPMI 1640, supplemented with 10% FCS and 1% PS. Cells were maintained at 37°C and 5% CO_2.
For uptake and biological response (i.e., viability and cell death) experiments, cells were treated with different activity concentrations of ^{177}Lu-DOTATATE as detailed below.
Lu-Mark was purchased from IDB Holland, and ^{177}Lu-DOTA-TATE was synthesized in-house according to a standard labeling procedure as used for patient treatment (molar activity 53 MBq/nmol, radiochemical yield >98% and radiochemical purity >95%).
X-ray treatment (at 86 keV) was delivered using a RS320 cabinet irradiator (X-Strahl) at a constant dose rate of 1.6 Gy/min.

Uptake data analysis and assumptions

Uptake and excretion assay

GOT1 and NCI-H69 cells were incubated with ^{177}Lu-DOTA-TATE (GOT1: 0.05 MBq/mL (0.10×10^{-8} M), 0.25 MBq/mL (0.48×10^{-8} M), 1 MBq/mL (1.9×10^{-8}M); NCI-H69: 0.1 MBq/mL (0.19×10^{-8} M), 0.25 MBq/mL (0.48×10^{-8} M), 1 MBq/mL (1.9×10^{-8}M)) for 4h in suspension (2×10^5 cells/mL in 5 mL culture medium). Cells were washed in PBS + 0.5% bovine serum albumin (BSA) twice by centrifugation and resuspension.

For uptake assays, the membrane-bound fraction of activity was dissociated in 50 mM glycine (Sigma-Aldrich) and 100 mM NaCl (Sigma-Aldrich) in dH_2O (pH 2.8) for 10 min. Subsequently, cells were separated as the internalized fraction of activity. Membrane and internalized fractions were measured separately on a 1480 WIZARD automatic γ-counter (Perkin Elmer). Uptake measurements were corrected for the number of cells after washing steps using a separate sample for cell counting.
For excretion assays, cells were seeded in 12-well plates at 2×10^5 cells/well and incubated for 0h, 4h, 24h, 36h, 72h (GOT1) or 0h, 24h, 48h, 96h, 128h (NCI-H69). At each corresponding timepoint, cells and medium were collected and separated by centrifugation, after which cell and medium fractions were measured separately on a γ-counter to determine the excreted activity.
Gamma counter measurements were corrected for decay and the uncertainty on estimated activity fractions in the different cell compartments was calculated as one standard deviation (SD) of 3 independent experiments, each performed in triplicate.

Proliferation assay

For NCI-H69 cells, the cellular proliferation rate was experimentally determined to correct for cell proliferation during incubation and to evaluate the cellular absorbed dose. Cells were incubated with ^{177}Lu-DOTA-TATE (0.1 MBq/mL (0.19x10-8 M), 1 MBq/mL (1.9x10-8 M) or vehicle) for 4h in suspension (2×10^5 cells/mL in 10 mL culture medium). Afterwards, cells were washed in PBS and seeded in 12-well plates (2×10^5 cells/well). After 0, 2, 4 and 6d, cells were collected, cell clumps were dissociated using

Trypsin-EDTA (0.25%) and cells were counted using a Countess automated cell counter (Thermo Fisher Scientific). Experiments were performed as 2 independent experiments, each performed in triplicate.

Receptor expression assay

GOT1 cells were fixed in 70% EtOH for at least 15 minutes at room temperature (RT). For $SSTR_2$ staining, cells were permeabilized in PBS + 1% Triton x-100 for 10 min on ice. Cells were washed with PBS + 1% BSA and incubated with primary antibody for $SSTR_2$ (Abcam, ab134152, 1:100) at RT for 90 min. Cells were washed in PBS + 0.1% Triton x-100 and incubated with secondary antibody Alexa FluorTM 594 goat anti-rabbit (Invitrogen, A11012, 1:1000) at RT for 60 min in the dark. Samples were washed and resuspended in PBS. Fluorescent signal was detected by flow cytometry on a LSRFortessa flow cytometer (BD Biosciences). Gating and analysis were performed using FlowJoTM software (BD Biosciences).

Heterogeneous activity distribution assumptions for GOT1 cells

We modeled heterogeneous activity distributions using two approaches: a lognormal distribution (μ = log(1), σ = 0.05) to represent random variability in receptor expression, as derived from flow cytometry data (Supplemental Figure 1), and a reduced uptake in the cluster center beyond three cell layers (*1*).For the latter, reduced uptake values were scaled based on the density of neighboring cells, calculated as the number of neighbors divided by the area of a circle with a defined "search radius." The masked image contours, which delineate single cells or the outermost cluster layers, were used to spatially define cells with maximum uptake values. Supplemental Figure 2 illustrates representative uptake fraction images, highlighting the effects of cluster formation on spatial activity distribution.

Viability assay

For PRRT, cells were treated in suspension with an activity concentration range (0.05 MBq/mL, 0.1 MBq/mL, 0.25 MBq/mL, 0.5 MBq/mL, 1.0 MBq/mL or vehicle) for 4h in 1 mL culture medium ($2x10^5$ cells/mL). For EBRT, cells were irradiated (GOT1: 0.5, 1, 2, 4 Gy; NCI-H69: 1, 2, 3, 4 Gy) under similar experimental conditions (brief EBRT exposure of cells in suspension at $2x10^5$ cells/mL after 4h incubation). After irradiation, cells were washed, plated (with 40000 cells/mL for NCl-H69 and 150000 cells/mL for GOT1) in triplicate in white-walled, round, flat bottom polystyrene 96-well plates (Corning) and incubated the following 7 days. Next, 100 µL of CellTiterGlo® 2.0 assay reagent (Promega) was added to each well, after which plates were incubated for 10 min at RT. CellTiter-Glo quantifies ATP levels, providing a measure of metabolically active cells. Luminescence was recorded using a Spectramax iD3x microplate reader (Molecular Devices) without wavelength selection. All raw luminescence values were normalized to the values of cells untreated to calculate cell viability. Experiments were performed as 3 independent experiments, each performed in triplicate.

Microscopic image collection and analysis

Immunofluorescent staining

GOT1 cells grown on a glass coverslip were fixed in 2% paraformaldehyde in PBS for 15 min. Cells were permeabilized in PBS + 1% Triton X-100 and blocked in PBS + 0.5% BSA + 20 mM glycine for 30 min. Samples were incubated with primary antibody for $SSTR_2$ (Abcam, ab134152, 1:250) in blocking buffer at RT for 90 min. Cells were washed in PBS + 0.1% Triton X-100 and incubated with Alexa FluorTM 594 goat anti-rabbit (Invitrogen, A11012, 1:1000) in blocking buffer at RT for 60 min. Samples were mounted using Vectashield containing DAPI (Vector Laboratories, H-1200). Imaging of $SSTR_2$ was performed on a TCS SP5 confocal microscope (Leica) using Z-stack acquisition. For the imaging, a 40x oil immersion objective and

405 nm (DAPI) and 561 nm ($SSTR_2$) lasers were used. A sample image is reported in Supplemental Figure 3.

Image analysis

A sample of the analyzed images for GOT1 and NCI-H69 cells is shown in Figures S4-S5. Background subtraction and edge detection (via Sobel operators) were performed to identify cell boundaries. Clusters and single cells were distinguished based on cell dimensions, and masks were created to define areas occupied by clusters and single cells. Spatial parameters, including distances, placements, and occupied areas, were analyzed and used as inputs for realistic cellular setups of floating and plated cells.

S-value simulations

Geant4 settings

The radioactive source was sampled using the predefined ion source definition (ENSDF database), which includes all the spectral components of ^{177}Lu. The Livermore (low-energy electromagnetic model) physics list was adopted.

The chemical composition of the cell nucleus, under normoxic conditions, was assumed to follow ICRU recommendations for typical cells (ρ = 1 g/cm³), while the cytoplasm was considered as made of water (ρ = 1 g/cm³) and the cell membrane as lipid (ρ = 0.92 g/cm³). The radionuclide was considered to be uniformly distributed in medium, cell membrane or cytoplasm. The target was the nucleus in all the simulations. The number of particles run per simulations ensure a relative error below 1 %.

Absorbed dose calculations

Dynamic transition modeling for absorbed dose calculations

To model the dynamic transition between uptake and decay phase for GOT1 cells (i.e., the dose rate change from a 3D floating scenario to a 2D plated exposure) a logistic function with a steepness parameter of k = 0.8 h^{-1} was employed as follows:

$$W(t) = \frac{1}{\left(1+e^{(-k\,(t-T_{mid})}\right)} \quad \text{(Eq. 1)}$$

with

$$T_{mid} = T_{uptake} - \frac{T_{transition}}{2}$$

This function quantifies the transition weight according to the time elapsed from the conclusion of the uptake phase (T_{uptake} = 4h) and extends over a transition period of $T_{transition}$ = 3h (ending at 7h). These weights are then used to perform a weighted average between uptake and decay phase, allowing for a smoother representation of the dose rate.

Error propagation and statistics

The absorbed dose rate error was determined by propagating uncertainties from activity measurements in the uptake and excretion assays, as the S-value errors were negligible under the assumption of constant cell size and nucleus density.

The error on the extrapolated activity data, was evaluated using the average relative error at each time point from the known uptake and decay measurements. The difference between the areas under the dose rate error bounds was used to calculate the uncertainty in absorbed doses.

To assess the normality of the absorbed dose dataset for GOT1 cells, the Shapiro-Wilk test was utilized. Best fitting models were chosen based on the Akaike Information Criterion test. The goodness of the fitting was evaluated by coefficient of determination ($R^2 > 0.7$).

Supplemental modelling information

Activity comparison

The internalized activity per cell was 5 to 7 times greater than membrane-bound activity for both cell lines. Additionally, the total internalized activity was on average 2.4±0.8 higher for NCI-H69 cells compared to GOT1 cells.

Medium and in-cluster cross-dose as primary dose contributors during incubation

Medium and in-cluster cross-dose as primary dose contributors in GOT1 floating phase

During the 4-hour uptake phase, GOT1 cells were exposed to radiation from three primary sources: (1) the clusters to which they belong (in-cluster cross dose), (2) clusters outside their own (cross-cluster absorbed dose), and (3) the surrounding medium.

The self-absorbed dose S-value from the membrane to the cell nucleus was 0.390 ± 0.001 mGy Bq^{-1} s^{-1}, and from the cytoplasm it was 0.482±0.001 mGy Bq^{-1} s^{-1}.

The 'in-cluster' contribution to the total cross S-value for cells placed either in the center or the edge of the cluster followed a saturation profile (Eq. 2, Supplemental Figure 7). The maximum value B_{max}, was $2.34x10^{-3}$±$7.98x10^{-5}$ Gy Bq^{-1} s^{-1} for cells at the center and $0.8834x10^{-3}$± $3.01x10^{-5}$ Gy Bq^{-1} s^{-1} for cells at the edge, with a half saturation constant (k_s) with respect to the number of cells (n) of 30±2 and 13±2 cells, respectively. These values were independent of the source localization (i.e., cell membrane or cytoplasm).

$$S_{in-cluster} = \frac{B_{max}\, n}{(k_s + n)} \quad \text{(Eq. 2)}$$

During the 4-hour uptake phase, the 'in-cluster' cross-absorbed dose per decay ranged from 0.18 to 0.37.

The S-value from the medium for both GOT1 and NCI-H69 was $2.36x10^{-12}$ Gy Bq^{-1} s^{-1}.

Effect of random cellular arrangement on cross dose in NCI-H69 floating phase

NCI-H69 cells remain suspended throughout the experiment, forming random 3D floating clusters. This necessitates an evaluation of how the increasing 'in-cluster' absorbed dose from randomly distributed daughter cells affects the overall dose assessment.

The self-absorbed dose S-value from the cell membrane was 1.79E0-4±9.60E-07 Gy Bq^{-1} s^{-1} and from the cytoplasm, it was $3.29x10^{-4}$±$1.30x10^{-6}$ Gy Bq^{-1} s^{-1}.

For both membrane and cytoplasm sources, a mono-exponential curve was fitted to the mean in-cluster cross S-value as a function of time (in days) for each initial cell count N_0. The fitting function used was:

$$S_{in-cluster}(t) = A\, e^{\gamma\, t}$$ (Eq. 3)

where A represents the initial value of S-cross (with N_0 cells) and γ represents the growth rate in days^{-1}. The corresponding plots are provided in Supplemental Figure 8.

To generalize the cross-cluster dose formula for NCI-H69, a linear regression was performed on the fitting parameters A and γ as functions of N_0 for both source locations. The determined parameters were:

$A = 4.67\ 10^{-8}\ N_0 + 1.76\ 10^{-4}$ Gy Bq^{-1} s^{-1}, $\gamma = 6.80\ 10^{-4}\ N_0 + 1.47\ 10^{-1}$ d^{-1} for cytoplasm

$A = 6.21\ 10^{-8}\ N_0 + 1.54\ 10^{-4}$ Gy Bq^{-1} s^{-1}, $\gamma = 5.80\ 10^{-4}\ N_0 + 1.45\ 10^{-1}$ d^{-1} for cell membrane

The cross S-values, weighted by the initial cluster size frequency, are detailed in Supplemental Table 2. These values were not significantly different (<1 %) from those obtained by matching the cluster size frequency daily (which accounted for the presence of larger clusters). This is likely because the cell population was predominantly organized into small clusters and single cells, causing the self-dose to outweigh the cross dose.

Cross-cluster contributions and dose rate heterogeneity in GOT1 plated phase

Significant cross-cluster and -single cell dose contributions in GOT1 plated phase

The in-cluster contribution of the highly packed (HFC) cell bi-layer to the total cross S-value followed a saturation profile (Supplemental Figure 9). The maximum S-value (B_{max}) was 2.11Ex10^{-3}±1.17x10^{-4} Gy Bq^{-1} s^{-1} for cells at the center and 7.05x10^{-4}±2.61x10^{-5} Gy Bq^{-1} s^{-1} for cells at the edge, with k_s of 27±6 and 10±2 cells, respectively. These values were independent of the source localization (i.e., cell membrane or cytoplasm). The HFC packing model, which neglected the 2D cross-cluster contribution and the complexity of cluster shapes, significantly underestimated the cross-dose by 66% for membrane sources and 90% for cytoplasm sources.

Dose rate heterogeneity: two distinct absorbed dose groups in 2D cluster forming cells

The absorbed dose values across GOT1 cells for each added activity did not follow a normal distribution ($p = 0.0205$). Given this, and assuming the existence of two distinct subpopulations (single isolated cells or cells in small clusters, and cells in larger clusters), we employed a bimodal distribution using a Gaussian Mixture Model (GMM). This approach provided a significantly better fit to the data (higher log-likelihood), closely followed the empirical density, and provided a more accurate representation of the absorbed dose variability compared to a single Gaussian model (Supplemental Figure 10).

Supplemental Figures

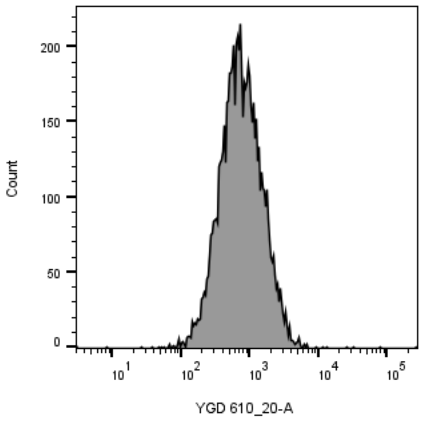

SUPPLEMENTAL FIGURE 1. Flow cytometry data of receptor expression in GOT1 cells. The minimal spread in fluorescence intensity indicates nearly homogeneous receptor expression across the cell population, from which the parameters of the lognormal distribution ($\mu = \log(1)$, $\sigma = 0.05$) were derived.

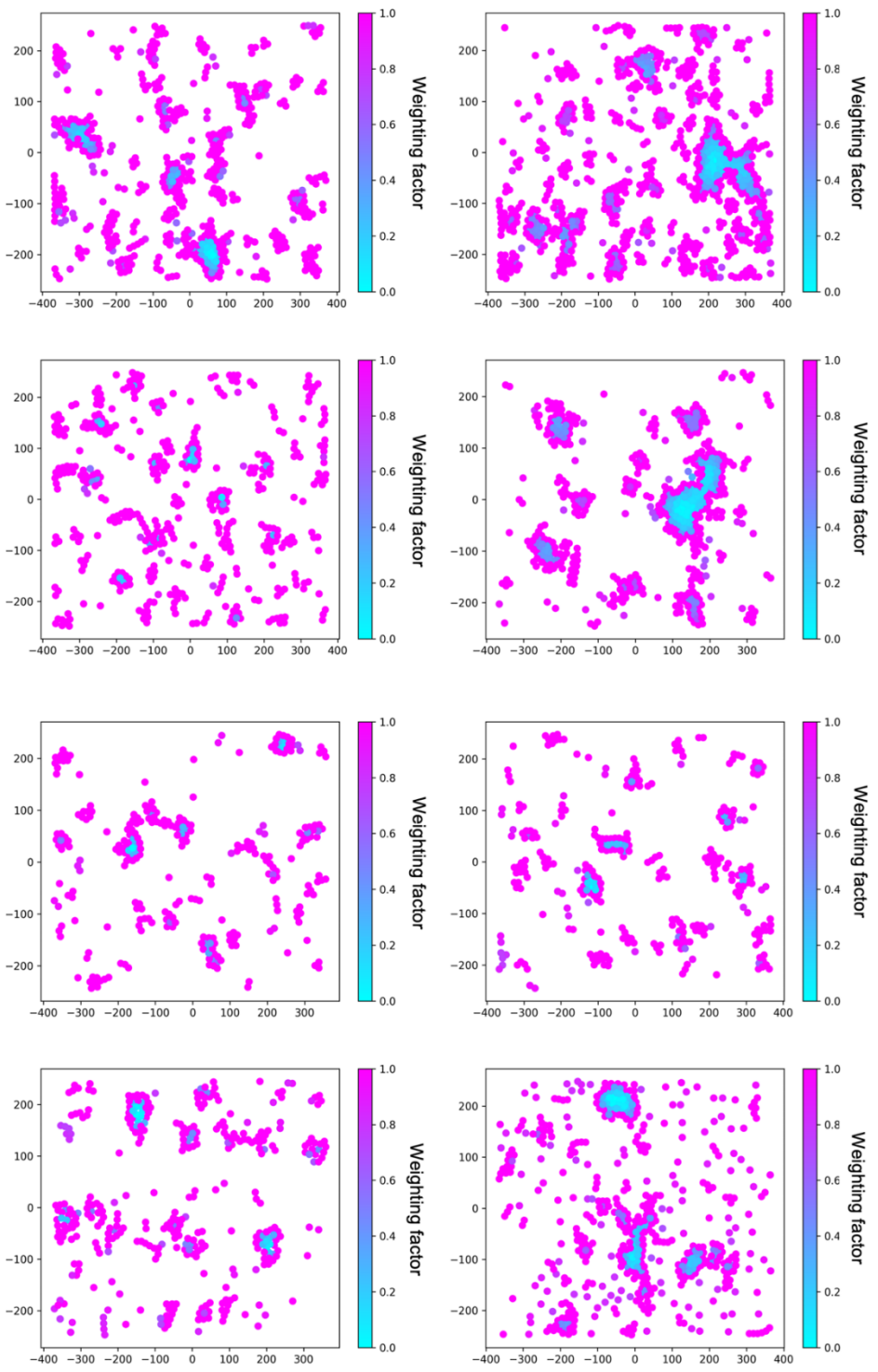

SUPPLEMENTAL FIGURE 2. Spatial representation of cell-plated setups colored based on uptake weighting factors to account for cluster formation. The color scale indicates the weighting factors, with cells having a value of 1 taking up activity without adjustment, while values <1 represent reduced uptake. Cells nearer to the center of larger clusters show lower uptake fractions due to increased density and cross-cluster interactions, reflecting reduced radionuclide availability in densely packed regions.

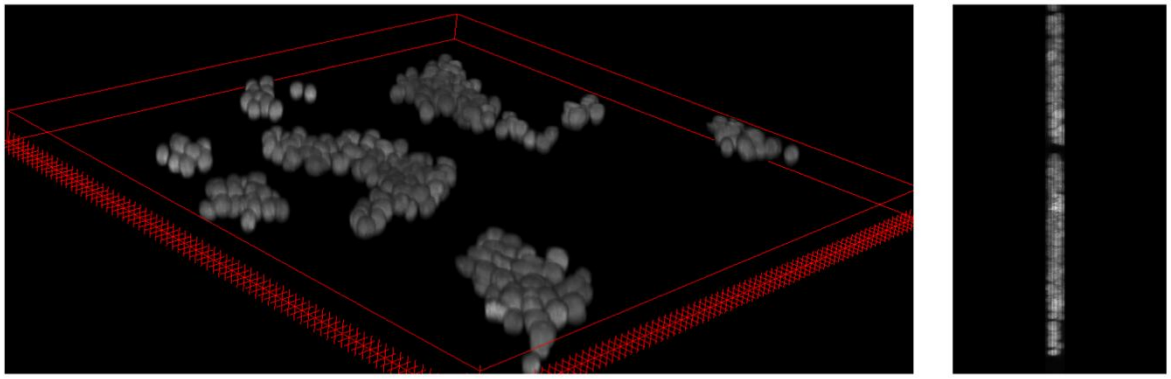

SUPPLEMENTAL FIGURE 3. Representative DAPI-stained nuclei of GOT1 cells in a plated setup, visualized in 3D to assess clustering behavior. The side view reveals the bilayer structure formed by the cells, enabling the determination of the number of layers within clusters for realistic modeling of spatial configurations in cellular dosimetry.

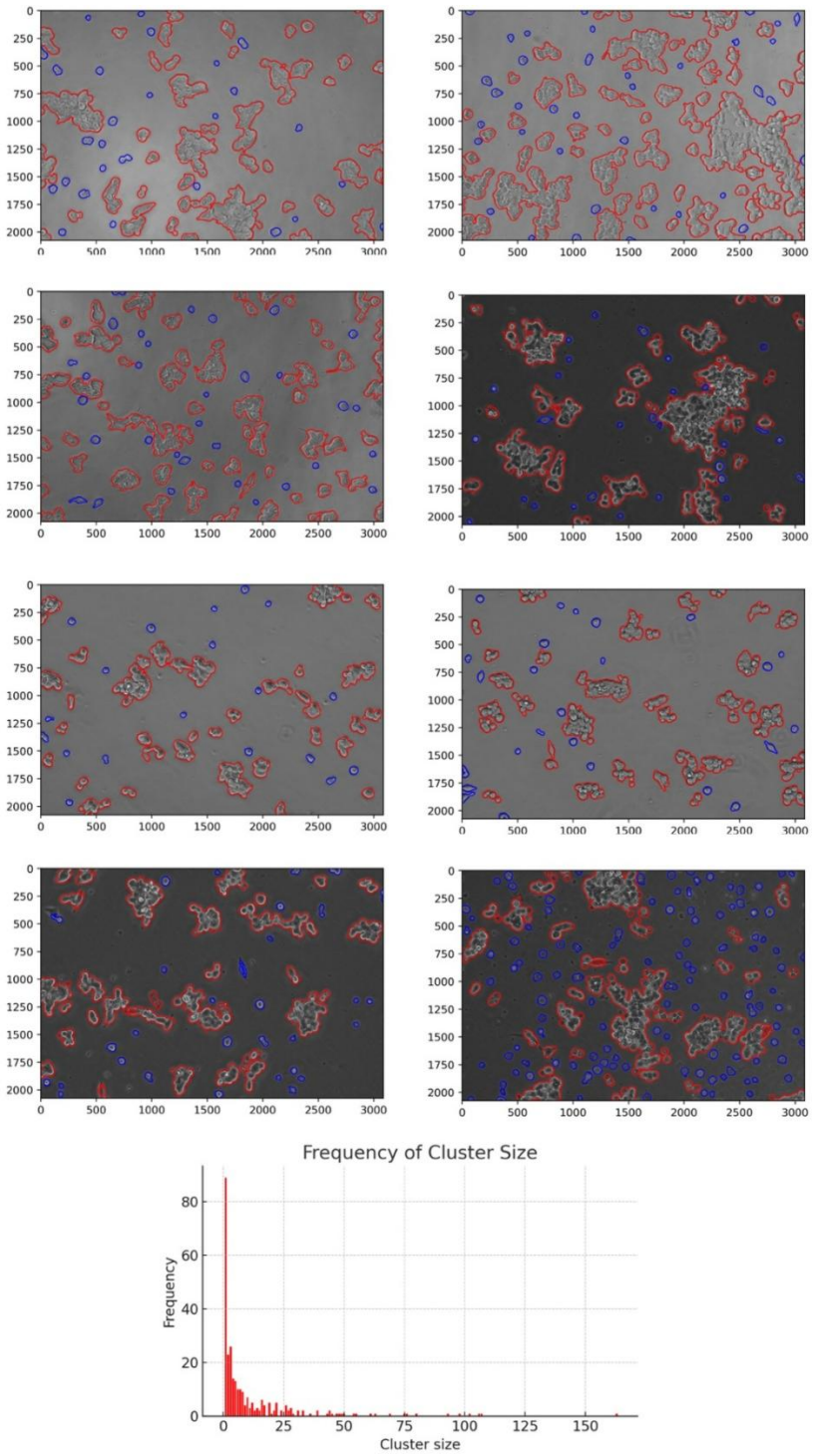

SUPPLEMENTAL FIGURE 4. Brightfield images of cell-plated setups (GOT1) with single cells (blue contours) and clusters (red contours) identified using image analysis. The automated detection process distinguishes individual cells from clusters, enabling spatial characterization, including cluster area and distances between cells and clusters, for realistic cellular dosimetry modeling. The accompanying histogram shows the frequency distribution of cluster sizes obtained from all analyzed images.

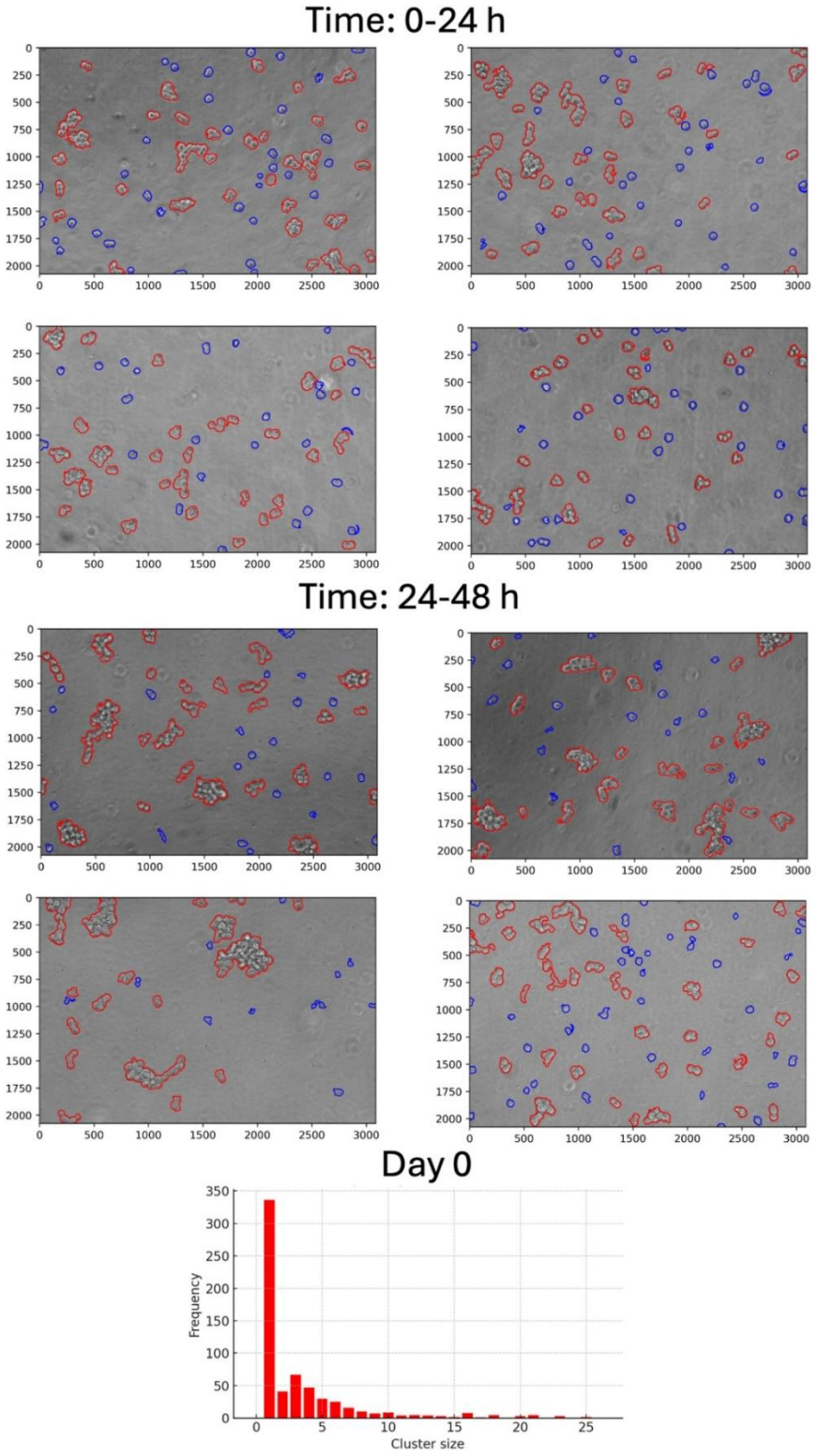

SUPPLEMENTAL FIGURE 5. Representative brightfield images at day 0 and 1 (before proliferation significantly reduces the bound activity per cell) of centrifuged NCI-H69 cells with single cells (blue contours) and clusters (red contours) identified using image analysis. The accompanying histogram displays the frequency distribution of cluster sizes at time 0, used for absorbed dose calculations.

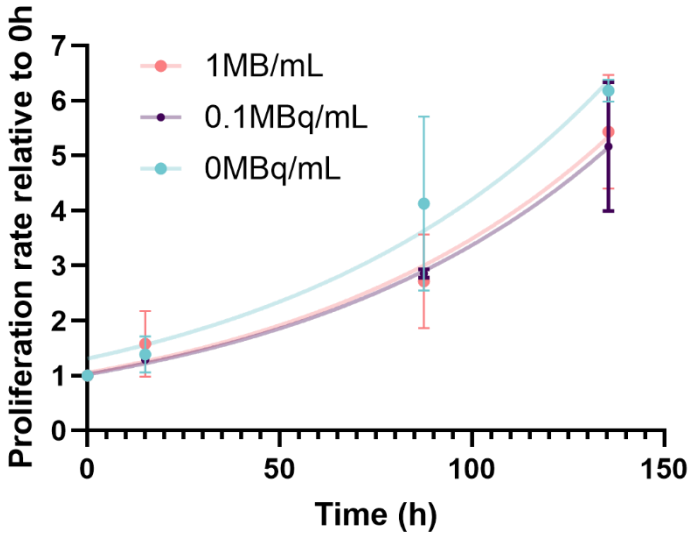

SUPPLEMENTAL FIGURE 6. Proliferation rates of NCI-H69 cells fitted with exponential growth curves to estimate doubling times depending on initial activity concentration. Error bars represent standard deviations.

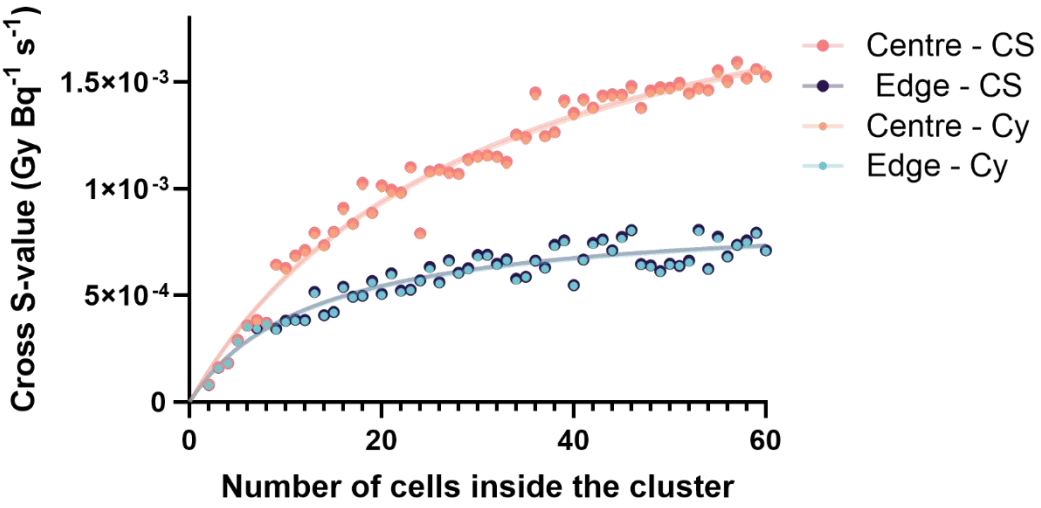

SUPPLEMENTAL FIGURE 7. Saturation profile of the 'in-cluster' cross S-value for floating compact cell clusters of GOT1 cells. The profiles were fitted using Equation 2, depending on source localization (Cy = cytoplasm, CS = Cell Surface) and cell target placement (center or edge). Error bars, representing standard deviations, are negligible due to the large number of particles in the Monte Carlo simulations.

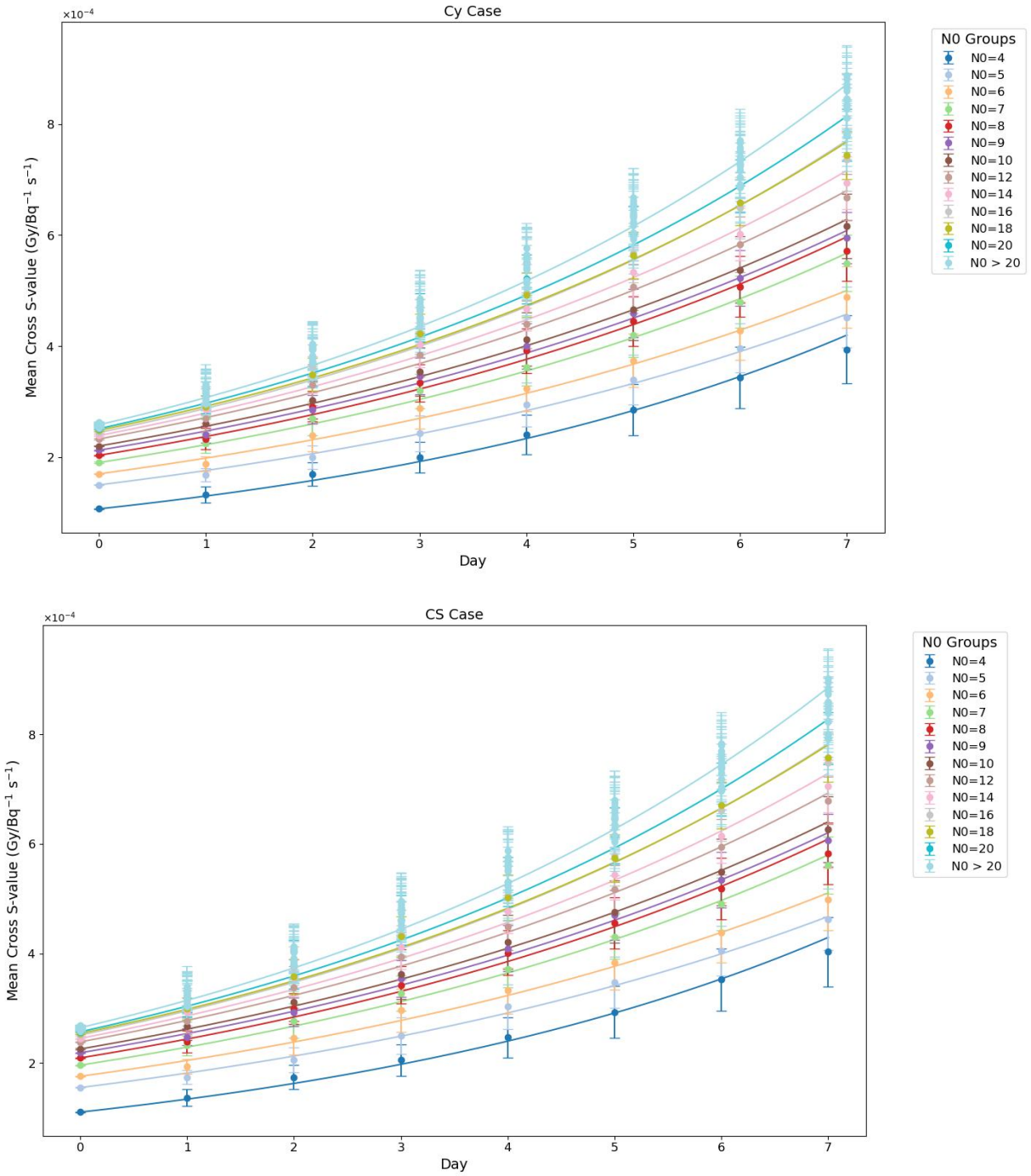

SUPPLEMENTAL FIGURE 8. Mean in-cluster cross S-values over time for NCI-H69 cells, grouped by initial (compact) cluster size (N_0). To reduce curve overlap, N_0 values are displayed in larger steps beyond N_0=10. Errors are shown as standard deviations (SD). Results are shown separately for source location in the cytoplasm ("Cy Case") and cell surface ("CS Case").

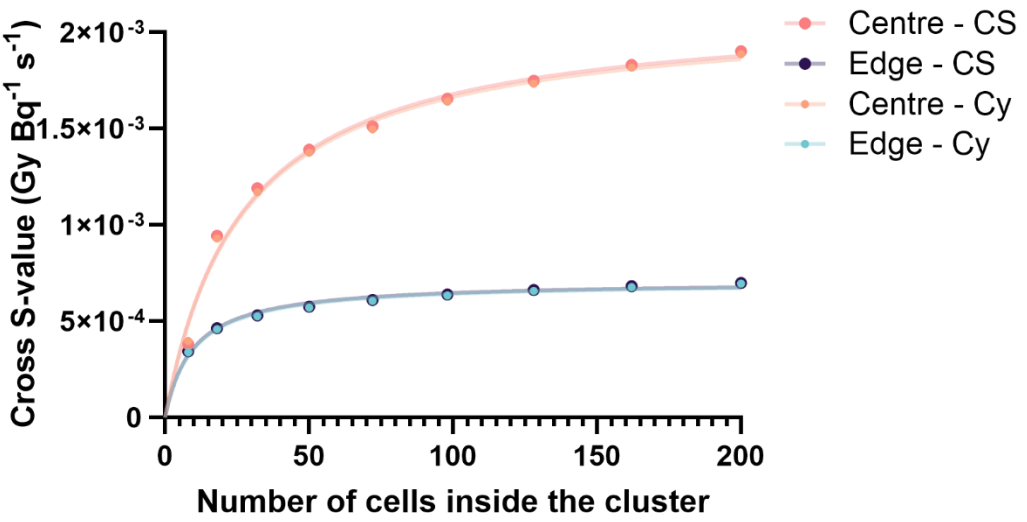

SUPPLEMENTAL FIGURE 9. Saturation profile of the 'in-cluster' cross S-value for plated bilayer compact cell clusters of GOT1 cells. Profiles are fitted using Equation 2, with distinctions based on source localization (Cy = cytoplasm, CS = cell surface) and cell target placement (center or edge). Error bars, representing standard deviations, are negligible due to the large number of particles in the Monte Carlo simulations.

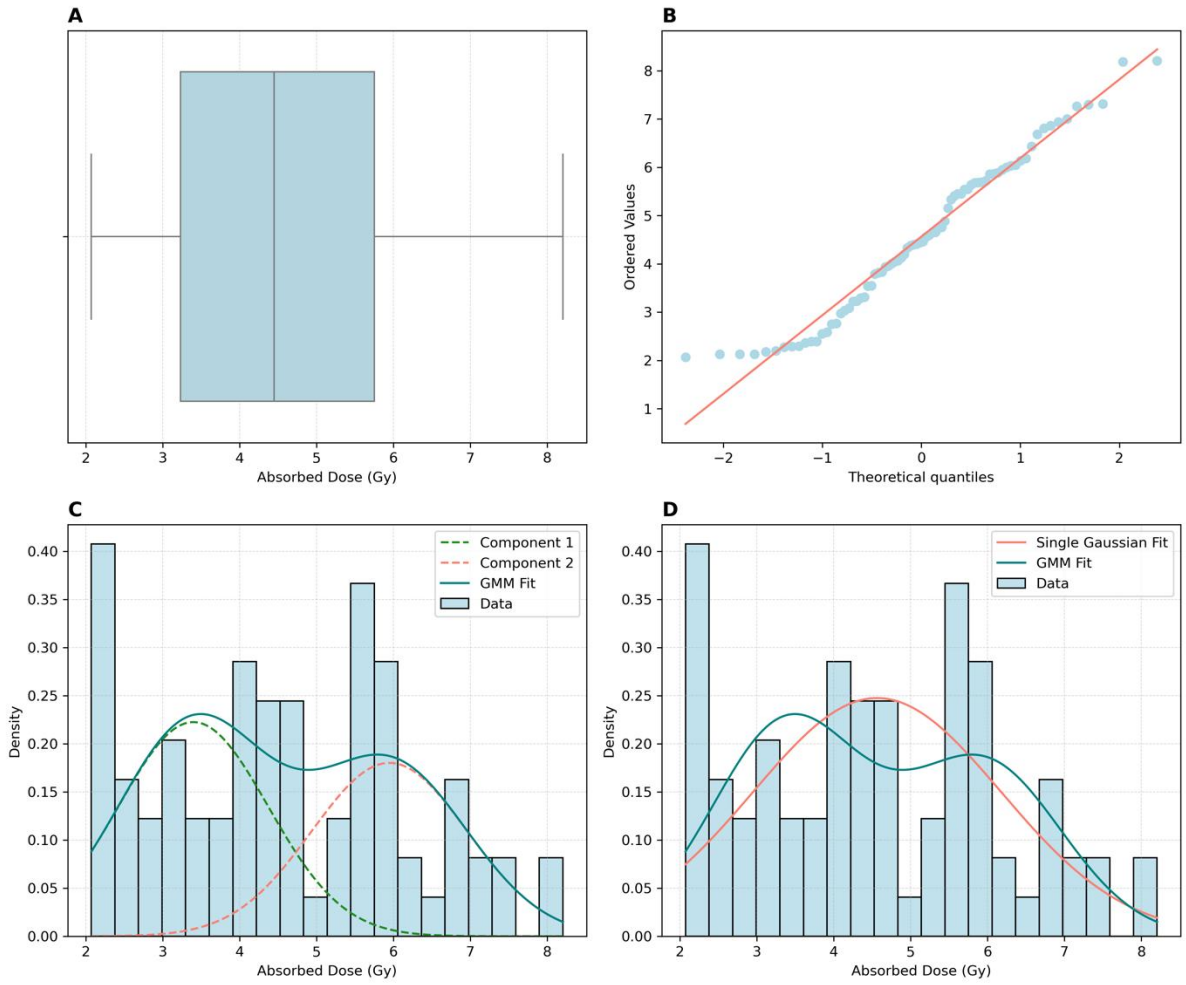

SUPPLEMENTAL FIGURE 10. Summary of absorbed dose distribution analysis at 1MBq/mL in GOT1 plated cells. (A) Box plot of absorbed dose values showing the median, interquartile range, and outliers. (B) Q-Q plot comparing the absorbed dose distribution to a theoretical normal distribution, with deviations indicating non-normality. (C) Histogram of absorbed dose values with Gaussian Mixture Model (GMM) fit (blue line) and its two components (dashed lines). (D) Comparison of the GMM fit (blue line) with a single Gaussian fit (red line), highlighting the improved fit provided by the GMM.

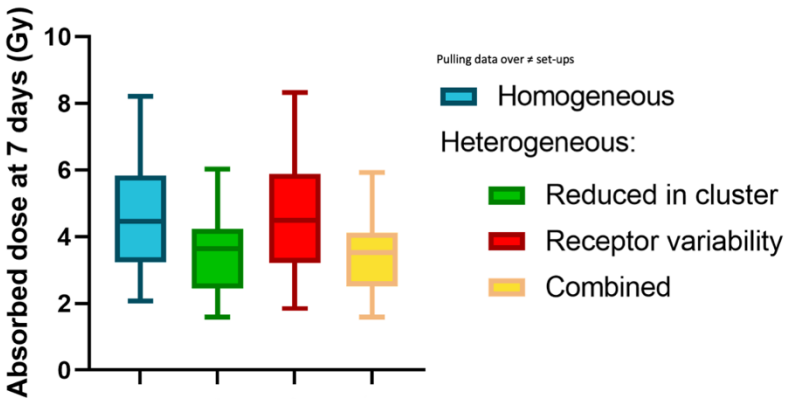

SUPPLEMENTAL FIGURE 11. Impact of heterogeneous activity assumptions on absorbed dose compared to homogeneous distribution. Reduced cluster uptake decreases absorbed dose by 0.5–1.1 Gy, while receptor heterogeneity has minimal impact on average absorbed dose.

Supplemental Tables

Supplemental Table 1. Uptake (and plateau) activity levels for GOT1 and NCI-H69 cells at different initial activity concentrations. The table reports the internalized and membrane-bound uptake activity with associated standard deviations for each initial activity concentration. Additionally, for GOT1 cells, the plateau level of activity is provided along with its standard deviation, as the internalized and membrane-bound activity stabilizes at approximately half of the initial uptake values. In contrast, for NCI-H69 cells, no plateau is reported since the activity is almost entirely excreted, with plateau levels 30–40 times lower than the initial uptake.

GOT1					
Initial Activity Concentration (MBq/mL)	**Location**	**Uptake Activity (Bq/cell)**	**SD (Bq/cell)**	**Plateau (Bq/cell)**	**SD (Bq/cell)**
1	Internalized	1,34E-02	5,97E-04	6,77E-03	3,15E-04
	Membrane	2,54E-03	8,54E-04	1,28E-03	3,85E-04
0.5	Internalized	1,20E-02	6,22E-04	6,14E-03	3,15E-04
	Membrane	2,12E-03	6,88E-04	1,10E-03	3,95E-04
0.25	Internalized	1,14E-02	7,50E-04	5,82E-03	3,85E-04
	Membrane	1,91E-03	6,92E-04	1,00E-03	3,50E-04
0.1	Internalized	7,55E-03	3,91E-04	3,91E-03	3,10E-04
	Membrane	1,15E-03	3,75E-04	6,10E-04	4,15E-04
0.05	Internalized	6,29E-03	2,80E-04	3,28E-03	1,70E-04
	Membrane	9,03E-04	2,48E-04	4,80E-04	1,15E-04

NCI-H69			
Initial Activity Concentration (MBq/mL)	**Location**	**Uptake Activity (Bq/cell)**	**SD (Bq/cell)**
1	Internalized	2,97E-02	3,78E-03
	Membrane	6,40E-03	8,34E-04
0.5	Internalized	2,81E-02	2,65E-03
	Membrane	5,87E-03	4,68E-04
0.25	Internalized	2,73E-02	2,10E-03
	Membrane	5,61E-03	4,16E-04
0.1	Internalized	1,97E-02	2,65E-03
	Membrane	4,01E-03	4,68E-04
0.05	Internalized	1,72E-02	2,65E-03
	Membrane	3,48E-03	4,68E-04

Supplemental Table 2. Mean cross S-values for NCI-H69 cells, used in absorbed dose calculations. The values are shown based on source localization on the cell surface (CS) and in the cytoplasm (Cy), with their respective standard deviations (SD). The cross S-values were evaluated based on the number of cells determined by proliferation. Weighting was performed using the initial cluster size frequency at day 0, which remained consistent across all days. This approach was consistent with an alternative method in which "clumping effects" were incorporated by weighting Scross based on the frequency distribution of cluster sizes at day 0,1,3,4,6. Specifically, the cluster size frequencies (±1 cell) were matched to the size of simulated data to obtain corresponding Scross values. For clusters with multiple matches, Scross values from later days were preferred to ensure randomness, as day 0 clusters are tightly packed.

Day	Mean Cross S-value from CS (Gy Bq^{-1} s^{-1})	SD (Gy Bq^{-1} s^{-1})	Mean Cross S-value from Cy (Gy Bq^{-1} s^{-1})	SD (Gy Bq^{-1} s^{-1})
0	2,66212E-06	4,97153E-09	2,57705E-06	4,7083E-09
1	3,04151E-06	6,53795E-08	2,94782E-06	6,27162E-08
2	3,90058E-06	1,38198E-07	3,7851E-06	1,31922E-07
3	4,69517E-06	1,7173E-07	4,56775E-06	1,6479E-07
4	5,55319E-06	2,0943E-07	5,4092E-06	2,02671E-07
5	6,47905E-06	2,6202E-07	6,32554E-06	2,53719E-07
6	7,54531E-06	2,92379E-07	7,37275E-06	2,82914E-07
7	8,63284E-06	3,16474E-07	8,45354E-06	3,0863E-07

Supplemental Table 3. Mean cross S-values for GOT1 cells plated after incubation, based on target cell location and setup, for membrane and cytoplasm sources. Columns correspond to different setups (1–8), with values provided for individual target locations (Targets 1–10), along with the average S_{cross} and relative standard deviation (SD).

Cell membrane (Gy Bq^{-1} s^{-1})	Set 1	Set 2	Set 3	Set 4	Set 5	Set 6	Set 7	Set 8
Target 1	4,28E-05	1,04E-03	9,12E-04	5,26E-04	7,43E-04	9,96E-04	6,13E-04	9,54E-04
Target 2	1,25E-03	2,76E-04	5,98E-04	9,13E-04	6,82E-04	5,67E-04	9,85E-05	8,59E-04
Target 3	9,71E-05	1,29E-03	4,61E-04	1,27E-03	1,14E-03	3,96E-04	1,07E-03	4,69E-04
Target 4	5,48E-04	1,48E-05	9,96E-04	1,48E-04	9,51E-04	2,98E-05	1,94E-04	1,38E-04
Target 5	6,32E-04	9,47E-04	7,29E-05	2,93E-05	6,59E-04	1,02E-03	6,18E-04	1,24E-03
Target 6	5,14E-04	3,95E-04	4,96E-04	6,67E-04	7,11E-05	4,67E-04	3,06E-05	1,03E-03
Target 7	1,90E-04	1,59E-03	3,16E-04	1,21E-03	5,05E-04	6,83E-04	9,11E-05	1,36E-03
Target 8	1,37E-03	9,57E-04	3,31E-04	7,09E-04	8,13E-04	7,05E-04	3,35E-04	1,37E-03
Target 9	2,47E-04	2,64E-04	1,04E-03	1,60E-03	8,78E-04	3,14E-04	1,00E-03	6,27E-04
Target 10	6,20E-04	1,08E-03	8,89E-04	5,31E-04	4,77E-05	8,89E-04	9,37E-04	6,68E-05
Average	5,51E-04	7,85E-04	6,11E-04	7,60E-04	6,49E-04	6,06E-04	4,98E-04	8,11E-04
Relative SD	78%	62%	52%	62%	52%	49%	77%	55%

Cell cytoplasm (Gy Bq^{-1} s^{-1})	Set 1	Set 2	Set 3	Set 4	Set 5	Set 6	Set 7	Set 8
Target 1	4,27E-05	1,03E-03	9,05E-04	5,23E-04	7,37E-04	9,90E-04	6,08E-04	9,46E-04
Target 2	1,25E-03	2,76E-04	5,95E-04	9,08E-04	6,77E-04	5,62E-04	9,83E-05	8,53E-04
Target 3	9,71E-05	1,28E-03	4,57E-04	1,27E-03	1,14E-03	3,93E-04	1,06E-03	4,66E-04
Target 4	5,43E-04	1,49E-05	9,88E-04	1,48E-04	9,44E-04	2,98E-05	1,94E-04	1,38E-04
Target 5	6,28E-04	9,41E-04	7,29E-05	2,93E-05	6,53E-04	1,01E-03	6,12E-04	1,23E-03
Target 6	5,11E-04	3,95E-04	4,94E-04	6,62E-04	7,11E-05	4,63E-04	3,07E-05	1,02E-03
Target 7	1,90E-04	1,59E-03	3,13E-04	1,20E-03	4,99E-04	6,78E-04	9,11E-05	1,35E-03
Target 8	1,36E-03	9,52E-04	3,28E-04	7,05E-04	8,06E-04	7,00E-04	3,34E-04	1,36E-03
Target 9	2,47E-04	2,63E-04	1,04E-03	1,59E-03	8,72E-04	3,11E-04	9,94E-04	6,24E-04
Target 10	6,16E-04	1,07E-03	8,83E-04	5,28E-04	4,75E-05	8,82E-04	9,31E-04	6,67E-05
Average	5,48E-04	7,81E-04	6,07E-04	7,56E-04	6,44E-04	6,02E-04	4,95E-04	8,06E-04
Relative SD	78%	62%	52%	62%	52%	49%	77%	55%

Supplemental Table 4. Dosimetric and biological response parameters for GOT1 cells, excluding medium contribution.

Added activity (MBq/mL)	Max. dose rate (range) (mGy/h)	T_0 (h)	K [/hour]	Avg. Absorbed dose at T_0 (Gy)	F_{min}	Min. eff. Dose Rate (range) (mGy/h)
1	53.67 (40.99-95.09)	168.11 ± 3.74	0.033 ± 0.005	4.58±0.41	0.47 ± 0.01	15.71 (6.75 - 28.82)
0.5	48.05 (36.79-84.97)	160.89 ± 2.43	0.026 ± 0.002	4.03±0.41	0.60 ± 0.01	14.58 (6.27 - 26.74)
0.25	45.23 (34.71-79.90)	155.54 ± 2.42	0.051 ± 0.007	3.63±0.4	0.71 ± 0.00	14.08 (6.06 - 25.82)
0.1	29.88 (23.00-52.69)	163.99 ± 157.97	0.273 ± 0.009	2.47±0.16	0.85 ± 0.01	8.99 (3.87 – 16.48)
EBRT	96000	168 - 208	0.006 - 0.0066	N.A.	N.A.	N.A.

Supplemental Table 5. Dosimetric parameters for NCI-H69 cells, excluding medium contribution.

Added Activity (MBq/mL)	Max Dose Rate ± SD (mGy/h)	Min Dose Rate ± SD at 7d (mGy/h)	Total Absorbed Dose (Gy)
1	39.01 ± 4.98	0.89 ± 0.09	1.45 ± 0.19
0.5	36.79 ± 3.42	0.84 ± 0.09	1.37 ± 0.19
0.25	35.68 ± 2.74	0.81 ± 0.09	1.32 ± 0.11
0.1	25.72 ± 3.42	0.59 ± 0.09	0.95 ± 0.13
0.05	22.4 ± 3.42	0.52 ± 0.09	0.82 ± 0.19

Supplemental Table 6 Average absorbed dose to nucleus per added activity of ^{177}Lu-DOTATATE for GOT1 and NCI-H69 cell lines at day 7, including medium contribution, and corresponding relative cell viability.

	Activity (MBq/mL)	Absorbed dose (Gy) ± SD (Gy)	Relative cell viability ± SEM
GOT1 cells	0	0	1.00 ± 0.06
	0.05	2.10 ± 0.16	0.90 ± 0.05
	0.1	2.55 ± 0.41	0.85 ± 0.03
	0.25	3.91 ± 0.41	0.83 ± 0.03
	0.5	4.23 ± 0.41	0.74 ± 0.03
	1	4.89 ± 0.41	0.74 ± 0.03
NCI-H69 cells	0	0	1.00 ± 0.02
	0.05	0.84 ± 0.19	0.91 ± 0.02
	0.1	0.98 ± 0.13	0.84 ± 0.02
	0.25	1.40 ± 0.11	0.88 ± 0.01
	0.5	1.53 ± 0.19	0.77 ± 0.00
	1	1.78 ± 0.19	0.67 ± 0.01

Supplemental Table 7 Average absorbed dose and fraction of alive cells for GOT1 cells at various activity concentrations and time points, excluding the contribution from the medium. The absorbed dose was calculated up to 14 days to align with cell death assessments, even though any dose delivered beyond 7 days is biologically ineffective due to the low dose rate. Figure 4C of the main paper illustrates the absorbed dose and survival trends for 0.25 and 1 MBq/mL, corresponding to this table. For NCI-H69 cells, all absorbed dose was delivered within 7 days and is reported in the main paper (Table 2).

Concentration (MBq/mL)	Time (hours)	Average absorbed dose (Gy)	Cell survival fraction	SD
0.05	96	1.46	N.A.	N.A.
	168	2.08	N.A.	N.A.
	264	2.65	N.A.	N.A.
	336	2.95	N.A.	N.A.
0.1	96	1.76	1.0	0.028
	168	2.51	0.89	0.109
	264	3.21	0.86	0.036
	336	3.56	0.84	0.093
0.25	96	2.69	0.99	0.028
	168	3.82	0.81	0.048
	264	4.87	0.72	0.104
	336	5.41	0.71	0.043
0.5	96	2.87	0.94	0.019
	168	4.07	0.78	0.052
	264	5.18	0.63	0.116
	336	5.75	0.60	0.093
1.0	96	3.22	0.95	0.061
	168	4.56	0.74	0.145
	264	5.79	0.48	0.077
	336	6.43	0.49	0.100

REFERENCES

1. Beltrán Hernández I, Rompen R, Rossin R, et al. Imaging of Tumor Spheroids, Dual-Isotope SPECT, and Autoradiographic Analysis to Assess the Tumor Uptake and Distribution of Different Nanobodies. *Mol Imaging Biol*. 2019;21:1079-1088.